Rarefied hypersonic flow simulations using the Navier-Stokes equations with non-equilibrium boundary conditions

Progress in Aerospace Sciences 52 (2012) 80–87

Rarefied hypersonic flow simulations using the Navier-Stokes equations with non-equilibrium boundary conditions

Christopher J. Greenshields[1] and Jason M. Reese[2]

[1] *OpenCFD Ltd, 9 Albert Road, Reading RG4 7AN, UK*
[2] *Dept. of Mechanical Engineering, University of Strathclyde, Glasgow G1 1XJ, UK*

21st July 2011

Abstract

This paper investigates the use of Navier-Stokes-Fourier equations with non-equilibrium boundary conditions (BCs) for simulation of rarefied hypersonic flows. It revisits a largely forgotten derivation of velocity slip and temperature jump by Patterson, based on Grad's moment method. Mach 10 flow around a cylinder and Mach 12.7 flow over a flat plate are simulated using both computational fluid dynamics using the temperature jump BCs of Patterson and Smoluchowski and the direct simulation Monte-Carlo (DMSC) method. These flow exhibit such strongly non-equilibrium behaviour that, following Patterson's analysis, they are strictly beyond the range of applicability of the BCs. Nevertheless, the results using Patterson's temperature jump BC compare quite well with the DSMC and are consistently better than those using the standard Smoluchowski temperature jump BC. One explanation for this better performance is that an assumption made by Patterson, based on the flow being only slightly non-equilibrium, introduces an additional constraint to the resulting BC model in the case of highly non-equilibrium flows.

1 Introduction

The aerothermodynamic design of hypersonic vehicles incorporates wind tunnel testing, flight experiments, and modelling and computer simulation. Computer simulation is particularly attractive due to its relatively low cost and its ability to deliver data that we cannot measure or observe, under conditions we cannot reproduce in a laboratory. Its efficacy relies upon the quality of the underlying numerical methods and physical modelling for the particular application.

The use of computational fluid dynamics (CFD) for aerothermodynamics of hypersonic vehicles is complex, compared to aerodynamics of automotive vehicles, for example. Flow discontinuities, high gradients and other flow features impose far greater demands on the underlying

numerical methods. Extreme temperatures require complex models for thermodynamics that might include non-equilibrium effects, radiation, and molecular dissociation and the modelling of chemical reactions. The changing constitution of the gas also affects diffusive and turbulent transport, which is difficult to model accurately.

A significant limitation is also due to an underlying assumption of the Navier-Stokes-Fourier (NSF) equations that the fluid is a continuum in local thermodynamic near-equilibrium. Where the gas density is low and/or where high density gradients exist, this assumption becomes less valid. To be precise, it is the modelling of momentum and energy transfer when gas molecules interact (diffusion) that is limited to near-equilibrium in the Navier-Stokes equations by the use of linear relationships between stress and strain-rate (Newton's viscosity law) and between heat-flux and temperature-gradient (Fourier's law), respectively. Furthermore, where the gas meets a solid body, boundary conditions (BCs) are required to model momentum and energy transfer through interaction of gas molecules with the solid surface. The no-slip and isothermal conditions, in which the fluid velocity and temperature are set to that of the solid surface, is similarly based on the assumption that the gas is in local thermodynamic equilibrium with the surface and is typically used in conjunction with the NSF equations.

To indicate the extent to which a gas is in local thermodynamic equilibrium, we define the Knudsen number,

$$Kn = \frac{\lambda}{L} \approx \frac{\lambda}{Q}\mathbf{l} \bullet \nabla Q \,, \tag{1}$$

where the molecular mean free path

$$\lambda = \sqrt{\frac{\pi}{2RT}}\frac{\mu}{\rho} \,, \tag{2}$$

L is a characteristic length scale of the fluid system, Q is a flow quantity of interest, such as the gas density ρ, pressure p or temperature T, and $\mathbf{l}$ represents a suitable spatial direction (generally the direction of greatest variation of Q). Wherever $Kn \lesssim 0.001$ in a flow, gas molecules undergo a large number of collisions over the typical length scale, and the conventional no-slip NSF equations are appropriate. As Kn rises, it is generally thought that the most significant departures from near-equilibrium occur at or near solid surfaces, where the use of non-equilibrium BCs offer improvement over no-slip, isothermal conditions. Further increases in Kn render the standard NSF equations for the gas inappropriate. One alternative is to turn to discrete particle methods, such as direct simulation Monte Carlo (DSMC), that provide a an approximation to the solution of the Boltzmann equation. Because it provides something closer to a solution of the Boltzmann equation itself, DSMC is the preferred method of solution at, for example, $Kn = 1$. However, the use of DSMC is severely limited by computational cost because $\Delta x, \Delta t \propto \lambda$ where Δx is the length of a computational cell and Δt is the time step for a given simulation. To a first approximation, a decrease in Kn of a factor of 10 requires decreases in cell volume, Δx^3, and Δt of 10^3 and 10 respectively, leading to a factor of 10^4 increase in simulation time. The practical use of DSMC becomes severely strained as Kn is reduced through the transition regime $0.001 < Kn < 1$.

There is therefore a practical need for continuum-based CFD for hypersonic flows within a particular range of Kn. Whether we use the NSF equations or more complex continuum

models, the BCs are a critical component of any such simulation. This is the subject of this paper, in which we review non-equilibrium BCs commonly proposed for hypersonic flows and investigate modifications to these BCs using test cases of hypersonic flow over a cylinder and a flat plate.

2 Standard non-equilibrium BCs

The classical BCs for non-equilibrium flow are the Maxwell model for velocity slip [1] and the Smoluchowski model for temperature jump [2]. For the velocity slip, Maxwell relies on a fairly descriptive derivation, beginning with the idea that the tangential momentum brought up to unit area of surface per second by approaching molecules is responsible for the tangential stress at the surface. He assumes that the approaching stream of molecules carries the same level of tangential momentum contained within the region of gas some distance away from the boundary. That gas consists of approaching and receding streams, each of which contribute to half of the stress within it. On striking the boundary, some fraction σ of the tangential momentum relative to the boundary surface is transferred from the molecules to the boundary. The gas must then slip in order that tangential momentum is conserved.

The tangential momentum balance includes contributions due to: (1) the shear stress $\boldsymbol{\tau}$; (2) the slip at the surface, calculated from the tangential slip velocity u_s and mean molecular speed $\bar{v}$; (3) thermal creep. The tangential momentum due to thermal creep is derived separately and accounts for the fact that hotter molecules have more momentum than colder molecules so lose proportionally more of it when they collide with a surface.

The Maxwell model is commonly expressed as:

$$u_s = A\left(\frac{2-\sigma}{\sigma}\right)\lambda\frac{\partial u_x}{\partial n} + \frac{3}{4}\frac{\mu}{\rho T}\frac{\partial T}{\partial x}\,, \tag{3}$$

where A is a constant of proportionality, x is the tangential direction, n is in the direction normal to the surface, pointing into the fluid, and μ is the viscosity. The second term on the right hand side relates to thermal creep.

By analogy with Maxwell's arguments for the momentum slip, the Smoluchowski model for temperature jump assumes the energy brought up to a boundary by approaching molecules per unit area of surface per second is responsible for the heat conducted through the boundary. On striking the boundary, the molecules give it some fraction α of the heat. The resulting model is usually expressed as:

$$T - T_w = \left(\frac{2-\alpha}{\alpha}\right)\frac{2\gamma}{(\gamma+1)\,\mathrm{Pr}}\lambda\frac{\partial T}{\partial n}\,, \tag{4}$$

where γ is the ratio of specific heats and Pr is the Prandtl number.

These expressions for the Maxwell and Smoluchowski BCs, given by Eqns 3 and 4, are typically adopted for hypersonic flows (if non-equilibrium BCs are used at all). In the authors' opinion, the equations are imprecise and misleading in the following ways.

First, Eqn 3 only specifies the tangential component of velocity and does not specify the normal component, which is the normal component of the surface itself and generally non-zero in the

case of a moving surface. It omits a reference surface velocity so that it is only valid for a stationary surface. This also creates the illusion that the equation is fundamentally different in form to Eqn 4.

Second, Maxwell originally related u_s to $\boldsymbol{\tau}$, which for a Newtonian fluid is

$$\boldsymbol{\tau} = \mu \left[\nabla \mathbf{U} + \nabla \mathbf{U}^{\mathrm{T}} - (2/3)\,\mathrm{tr}(\nabla \mathbf{U})\mathbf{I} \right], \tag{5}$$

where $\mathbf{U}$ is the velocity vector and $\mathbf{I}$ is the identity tensor. Eqn 3 incorporates the first of the terms on the right hand side of Eqn 5, but ignores the other terms. The second term equates to zero for a flat boundary surface, but when the surface is curved its inclusion is necessary, as demonstrated in the studies of a cylindrical Couette flow and drag on a sphere [3]. The third term is also clearly non-zero for compressible flows.

Finally, the way Eqns 3 and 4 are expressed, with the slip/jump value on the left hand side and the gradient and other terms on the right, gives the impression they are Dirichlet (specified value) BCs whose specified boundary values are calculated from the gradient and other terms. However they are Robin BCs, i.e. a weighted combination of Dirichlet and Neumann (specified normal gradient) conditions, which can be expressed as

$$\phi + a\,\mathbf{n} \bullet \nabla \phi = b\,, \tag{6}$$

where $\mathbf{n}$ is unit normal vector at the surface pointing *outwards* of the domain, ϕ is the dependent variable, and a and b are model coefficients. In this form, it is fairly clear that the BC represents a Dirichlet condition $\phi = b$ in the limit of $a \to 0$ and a Neumann condition $\mathbf{n} \bullet \nabla \phi = 0$ in the limit $a \to \infty$, but in general represents a condition between these extremes.

Where ϕ is velocity, a vector field, the Robin condition applies to the tangential component only, with the normal component being represented by a Dirichlet condition. The Robin condition can be reduced to a Dirichlet condition in the normal component by transformation of the normal gradient with tensor $\mathbf{S} = \mathbf{I} - \mathbf{nn}$, so that the Eqn 6 becomes:

$$\phi + a\,\mathbf{S} \bullet \nabla_{\mathbf{n}} \phi = b\,, \tag{7}$$

in which we introduce the shorthand $\mathbf{n} \bullet \nabla \equiv \nabla_{\mathbf{n}}$. Both slip and jump BCs can be expressed in the form of Eqn 7, although the transformation by tensor $\mathbf{S}$ may be omitted in the case of temperature jump since T is a scalar so is unaffected by the transformation.

3 Patterson's derivation of non-equilibrium BCs

The Maxwell-Smoluchowski BCs given by Eqns 3 and 4 are the most commonly used non-equilibrium BCs and most development of the BCs involves determining optimal values of model constant A and the accommodation coefficients σ and α. These coefficients are either determined empirically or calculated from kinetic theory, e.g. [4, 5].

Rather than optimise coefficients for these standard BC equations, in this work we have revisited an alternative derivation for non-equilibrium BCs based on Grad's moment method [6]. We attribute this alternative derivation to G. N. Patterson since it seems to appear first in

his book of 1956 [7]. It is based on integrals of mass, momentum and energy for incident and reflected molecules at a surface. It assumes diffuse reflections everywhere, so ultimately generates BCs for accommodation coefficients $\sigma, \alpha = 1$, although adaptation of the method for specular reflections is relatively trivial and is included in a later book [8].

The non-equilibrium BCs of Patterson appear in some significant work soon after their publication, notably in a study of hypersonic flow over a flat plate [9] in which velocity slip and temperature jump are analysed and discussed in detail, and in which mention is made of the existence of pressure jump. The method was also extended to produce a system of boundary conditions for a multicomponent mixture including concentration slip boundary conditions [10]. Despite that, Patterson's work seems to have been largely forgotten, so first we will reproduce the key elements of the derivation here using tensor notation.

Conservation equations for mass, momentum and energy between incident and reflected molecules are expressed in terms of integrals over molecular velocity $\mathbf{c}$. It is assumed that the incident molecules have a distribution function f that departs slightly from that of a Maxwellian distribution f_0, and the reflected molecules are assumed to have a Maxwellian distribution at the wall temperature T_w. From $\mathbf{c} = \mathbf{U} + \mathbf{C}$, where $\mathbf{C}$ is the peculiar velocity, the general distribution function f is expressed as an expansion into Hermite polynomials:

$$f = f_0 \left[1 + F(\mathbf{H})\right], \tag{8}$$

where $\mathbf{H} = \sqrt{2\beta}\mathbf{C}$ is a normalised peculiar velocity and $\beta = 3/(2\overline{\mathbf{C}\bullet\mathbf{C}}) = 1/(2RT)$, where R is the gas constant. Following Grad's method, $F(\mathbf{H})$ is approximated by a power series:

$$F(\mathbf{H}) = \mathbf{a}\bullet\mathbf{H} + \frac{1}{2}\mathbf{A}\,\vdots\,\mathbf{HH} + \frac{1}{6}\mathbb{A}\,\vdots^{3}\,\mathbf{HHH}\,, \tag{9}$$

where $\mathbf{a}$, $\mathbf{A}$, $\mathbb{A}$ are tensors of rank 1, 2 and 3 respectively and '$\vdots$' and '$\vdots^{3}$' represent the double and triple inner products, respectively. Both $\mathbf{A}$ and $\mathbb{A}$ are symmetric and two relationships between coefficients can be deduced from constraints on mean values of $\mathbf{H}$, i.e. $\mathrm{tr}(\mathbf{A}) = 0$; and $2\mathbf{a} + \mathbb{A}\,\vdots\,\mathbf{I} = 0$. The coefficients $\mathbf{a}$ and $\mathbf{A}$ are determined such that the distribution function reproduces the corresponding basic variables (averaged functions of $\mathbf{H}$) as its moments:

$$\mathbf{a} = -\frac{1}{p\sqrt{RT}}\mathbf{q}\,, \quad \mathbf{A} = -\frac{\boldsymbol{\tau}}{p}\,, \tag{10}$$

where $\mathbf{q}$ is the heat flux vector. The tensor $\mathbb{A}$ can be related to $\mathbf{a}$ such that for the purpose of developing expressions at a boundary, the following relations are satisfied:

$$\mathbb{A}\,\vdots^{3}\,\mathbf{nnn} = -\frac{6}{5}\mathbf{a}\bullet\mathbf{n}\,, \quad \mathbf{S}\bullet(\mathbb{A}\,\vdots\,\mathbf{nn}) = -\frac{2}{5}\mathbf{S}\bullet\mathbf{a}\,. \tag{11}$$

3.1 Mass conservation condition

The analysis of mass conservation arrives at the following equation:

$$\frac{\rho_w}{\rho} = \sqrt{\frac{T}{T_w}}\,(1+\zeta)\,, \tag{12}$$

where

$$\zeta = \frac{1}{2}\mathbf{A}:\mathbf{nn} = -\frac{\boldsymbol{\tau}:\mathbf{nn}}{2p} \tag{13}$$

is a ratio of the normal viscous stresses to pressure. The subscript w denotes properties of the fluid with an equilibrium distribution at the wall temperature T_w and those with no subscript are those of the actual fluid at the wall surface.

Eqn 12 is not really itself a BC, but an expression for density ρ_w of diffusely reflected particles that is used in the derivation of subsequent BCs. The expression accounts for the difference in molecular speeds of the incident and reflected particles, both in terms of mean speed (due to different temperatures) and distribution function.

3.2 Momentum conservation BCs

Conservation of momentum is split into tangential and normal momentum components leading to equations for velocity slip and pressure jump respectively. The tangential momentum balance equation produces [7, 8]:

$$\mathbf{U} + \frac{1}{2\sqrt{2\beta}(1+\zeta)}\left(-\frac{2-\sigma}{\sigma}\sqrt{2\pi}\mathbf{S}\bullet(\mathbf{A}\bullet\mathbf{n}) - \frac{2}{5}\mathbf{S}\bullet\mathbf{a}\right) = \mathbf{U}_w\,. \tag{14}$$

Substituting expressions for $\mathbf{a}$ and $\mathbf{A}$ from Eqn 10, Eqn 14 becomes

$$\mathbf{U} + \sqrt{\frac{\pi RT}{2}}\frac{1}{p(1+\zeta)}\frac{2-\sigma}{\sigma}\mathbf{S}\bullet(\boldsymbol{\tau}\bullet\mathbf{n}) + \frac{1}{5p(1+\zeta)}\mathbf{S}\bullet\mathbf{q} = \mathbf{U}_w\,. \tag{15}$$

Substituting into Eqn 15 the viscous stress tensor $\boldsymbol{\tau} = \mu\nabla\mathbf{U} + \boldsymbol{\tau}_{tr}$ where $\boldsymbol{\tau}_{tr}$ represents the second and third terms (transpose and trace respectively) on the right of Eqn 5, and applying the perfect gas law $p = \rho RT$, gives the slip condition for $\mathbf{U}$:

$$\mathbf{U} + a_{\mathbf{U}}\mathbf{S}\bullet(\mathbf{n}\bullet\nabla\mathbf{U}) = \mathbf{U}_w - \frac{a}{\mu}\mathbf{S}\bullet(\mathbf{n}\bullet\boldsymbol{\tau}_{tr}) - \frac{1}{5p(1+\zeta)}\mathbf{S}\bullet\mathbf{q}\,, \tag{16}$$

where the coefficient

$$a_{\mathbf{U}} = \frac{1}{1+\zeta}\frac{2-\sigma}{\sigma}\lambda\,. \tag{17}$$

Eqn 16 follows the general form for a slip BC of Eqn 7 in which, in addition to the wall velocity $\mathbf{U}_w$, the right hand side contains the term in $\boldsymbol{\tau}_{tr}$ which is non-zero in the case of a curved boundary (i.e. the curvature correction term discussed in section 2 and analysed previously [3]). The term in $\mathbf{q}$ is the thermal creep term, which can be expressed in terms of T by substituting expressions for Fourier's law of conduction, $\mathbf{q} = -k\nabla T$, the perfect gas law and Prandtl number $\mathrm{Pr} = \mu C_p/k$ as follows:

$$-\frac{1}{5p(1+\zeta)}\mathbf{S}\bullet\mathbf{q} = \frac{1}{5(1+\zeta)}\frac{\gamma}{(\gamma-1)\,\mathrm{Pr}}\frac{\mu}{\rho T}\mathbf{S}\bullet\nabla T\,. \tag{18}$$

The normal momentum balance results also in a jump condition for pressure as follows:

$$p\left(1+2\zeta+\frac{2-\sigma}{\sigma}\frac{4}{5\sqrt{2\pi}}\mathbf{a}\bullet\mathbf{n}\right)=p_w. \tag{19}$$

Eqn 19 for pressure jump is usually ignored in rarefied gas simulations, and even when it does appear, its use is unclear. Gupta et al. [10], for example, state that "...usually, the equation for pressure slip is not required as a boundary condition but is needed to obtain the surface pressure". By "surface pressure", they must mean p rather than p_w (which is the pressure of the fluid with an equilibrium distribution at the wall temperature T_w); p_w must be calculated from T_w, an input to the temperature jump BC, and ρ_w which can be calculated from Eqn 12.

3.3 Energy conservation BC

The analysis of energy conservation arrives at the following equation [7, 8], in which it is assumed $\mathbf{U}_w=\mathbf{0}$:

$$\beta\mathbf{U}\bullet\mathbf{U}\,(1+\zeta)+\sqrt{\frac{\beta}{2}}\mathbf{U}\bullet\left(-\frac{2-\sigma}{\sigma}\sqrt{2\pi}\mathbf{A}\bullet\mathbf{n}+\mathbb{A}\mathbf{:}\mathbf{nn}\right)$$
$$+2\left(1+\frac{3}{2}\zeta+\frac{1}{2}\sqrt{\frac{\pi}{2}}\frac{2-\alpha}{\alpha}\mathbf{a}\bullet\mathbf{n}\right)=2\left(\frac{\beta}{\beta_w}\right)^{3/2}\frac{\rho_w}{\rho}\,. \tag{20}$$

Combining Eqns 11, 14 and 20, and noting that $\mathbf{U}\bullet\mathbf{v}=\mathbf{U}\bullet(\mathbf{S}\bullet\mathbf{v})$ for any vector $\mathbf{v}$ since $\mathbf{n}\bullet\mathbf{U}=0$,

$$-\beta\mathbf{U}\bullet\mathbf{U}\,(1+\zeta)+2\left(1+\frac{3}{2}\zeta+\frac{1}{2}\sqrt{\frac{\pi}{2}}\frac{2-\alpha}{\alpha}\mathbf{a}\bullet\mathbf{n}\right)=2\frac{T_w}{T}(1+\zeta)\,. \tag{21}$$

Substituting Eqn 12 gives:

$$T\left(1+\frac{1}{2+3\zeta}\sqrt{\frac{\pi}{2}}\frac{2-\alpha}{\alpha}\mathbf{a}\bullet\mathbf{n}\right)=T_w\left(\frac{2+2\zeta}{2+3\zeta}\right)\left(1+\frac{1}{4RT_w}\mathbf{U}\bullet\mathbf{U}\right)\,. \tag{22}$$

Finally, introducing the expressions for Fourier's law, perfect gas and Prandtl number, the equation can be written:

$$T+a_T\nabla_{\mathbf{n}}T=T_w\left(\frac{2+2\zeta}{2+3\zeta}\right)\left(1+\frac{1}{4RT_w}\mathbf{U}\bullet\mathbf{U}\right), \tag{23}$$

where the coefficient

$$a_T=\frac{1}{2+3\zeta}\frac{2-\alpha}{\alpha}\frac{\gamma}{(\gamma-1)\,\mathrm{Pr}}\lambda\,. \tag{24}$$

3.4 Patterson's temperature BC

Eqn 23 follows the general form for a slip condition of Eqn 7, and yet Patterson takes the analysis further, first assuming $\mathbf{U} \bullet \mathbf{U} \ll 4RT$ then rearranging Eqn 20 to give:

$$\frac{T}{T_w} = 1 - \left(\frac{1}{2}\zeta + \frac{1}{2}\sqrt{\frac{\pi}{2}}\frac{2-\alpha}{\alpha}\mathbf{a}\bullet\mathbf{n}\right) \Big/ \left(1 + \frac{3}{2}\zeta + \frac{1}{2}\sqrt{\frac{\pi}{2}}\frac{2-\alpha}{\alpha}\mathbf{a}\bullet\mathbf{n}\right). \tag{25}$$

Patterson then assumes the denominator of the fraction on the right hand side is approximately unity, yielding:

$$T + a_T \nabla_{\mathbf{n}} T = T_w \left(\frac{2-\zeta}{2}\right), \tag{26}$$

where the coefficient

$$a_T = \frac{2-\alpha}{\alpha}\frac{\gamma}{2(\gamma-1)\,\mathrm{Pr}}\frac{T_w}{T}\lambda\,. \tag{27}$$

4 Mach 10 flow around a cylinder

We consider the hypersonic cross-flow of argon over a two-dimensional cylinder of radius $R = 152.4$ mm (6 inches) as shown in Fig 1. The selected test case is one used in a previous numerical study [11]. The freestream parameters are $T_\infty = 200$ K, $\mathbf{U}_\infty = (2624.1, 0, 0)$ m/s, $p_\infty = 47$ mPa. These flow parameters correspond approximately to Mach 10 and, taking the length scale as the cylinder diameter in Eqn 1, $Kn \approx 0.25$. The cylinder wall is held at a uniform temperature $T_w = 500$ K.

Our simulations were undertaken using OpenFOAM [12], the open source CFD toolbox. OpenFOAM includes solvers for continuum CFD that use the finite volume method, and solvers that use discrete/particle methods such as DSMC, all operating on an unstructured mesh of polygonal cells of any shape. The `dsmcFoam` application [13], was used for DSMC simulations on the same test case, using the variable hard sphere (VHS) model with temperature exponent $\omega = 0.734$, reference temperature $T_{\mathrm{ref}} = 1000$ K, molecular diameter $3.595{\times}10^{-10}$ m and mass $66.3{\times}10^{-27}$ kg. Particles that collide with wall surfaces are reflected diffusely, and the velocity slip and temperature jump are calculated based on the particles that strike the surface, according to relations used in the DS2V code of Bird [14]. The simulation used 11.9×10^6 equivalent particles, each representing 5.3×10^{10} argon atoms. The mesh consisted of 36,000 cells whose smallest size was approximately 2×2 mm. In this and subsequent simulations the number of cells (and the number of particles in DSMC) were set at a level where results fell within 1% of subsequent simulations on meshes with twice the number of cells.

The `rhoCentralFoam` application [15] was used to solve the Navier-Stokes equations with non-equilibrium BCs for continuum CFD with $\sigma = \alpha = 1$, which are equivalent to the diffuse reflections simulated in the DSMC solver. A power law model was used for viscosity, equivalent to the VHS model [11], of the form $\mu = \mu_{\mathrm{ref}}(T/T_{\mathrm{ref}})^\omega$, with $\mu_{\mathrm{ref}} = 50.7 \times 10^{-6}$ Pa s. The simulations used a mesh of 28,000 cells that were graded from $\Delta x, \Delta y \approx 4$ mm in the far-field to $\Delta x, \Delta y \approx 25\mu$m at the cylinder surface. Further refinement to this mesh and the DSMC mesh gave

4.1 Preliminary work

Initial simulations were undertaken using the momentum BC of Eqn 16 combined with, in turn, the energy BCs of Eqns 23 and 26. Initial simulations on this case suffered numerical instability, originating from the downstream side of the cylinder surface. The instability appears to be caused by the terms in ζ in the BC equations which, using the definition of n pointing *into* the domain in Eqn 3, and assuming the flow is locally trace-free, approximates to

$$\zeta \approx -\frac{\mu}{p}\frac{\partial u_n}{\partial n}. \tag{28}$$

It is clear that Eqn 12 is unphysical when $\zeta \leq -1$ and somewhat implausible when $\zeta > 1$. In previous work [7, 8, 10], it has been assumed that $|\zeta| \ll 1$, but in the case of rarefied, high speed flows this is not guaranteed. In this cylinder case, for example, $|\partial u_n/\partial n|$ is particularly high in the stagnation region and fairly high in the expansion region downstream of the cylinder. In the stagnation region, $\partial u_n/\partial n < 0$ so $\zeta > 0$ and p is quite high so $|\zeta|$ is not excessively high. However, in the downstream region $\partial u_n/\partial n > 0$ and because, p is small, it is certainly possible that $\zeta \leq -1$.

In our preliminary simulations on this case we evaluated ζ at the downstream side of the cylinder surface along the geometry centre line. Over a range of simulations, values in the range $-20 < \zeta < -10$ were measured. We therefore attributed the instability in the BCs to the unphysical nature of the equations when $\zeta \leq -1$. To make the BCs physical, we first considered clipping ζ when it fell below some level. Clipping would need to occur before ζ reached -1, but there is no obvious choice of clipping 'level'. Similarly, some clipping would probably be required beyond a positive level of ζ but, again, there is no obvious choice of level. Therefore, in the absence of any physical basis to choose clipping levels, we decided to set $\zeta = 0$. This setting was adopted for the remainder of the work presented in this paper. In addition, as Patterson's temperature BC, Eqn 26, was derived using the assumption $\mathbf{U} \bullet \mathbf{U} \ll 4RT$, we applied the same assumption to Eqn 23. This and the previous setting, $\zeta = 0$, reduces both Eqns 23 and 26 to:

$$T + a_T \nabla_{\mathbf{n}} T = T_w \,. \tag{29}$$

The 'energy conservation BC' of Eqn 23 thus reduces to a form of the Smoluchowski temperature BC in which

$$a_T = \frac{2-\alpha}{\alpha}\frac{\gamma}{2(\gamma-1)\,\mathrm{Pr}}\lambda \,. \tag{30}$$

In the remainder of this paper we refer to Eqn 29 with the coefficient a_T in Eqn 30 as the "Smoluchowski BC", and with the coefficient a_T in Eqn 27 (that includes an additional factor T_w/T) as the "Patterson BC".

4.2 Results

We ran CFD and DSMC simulations of Mach 10 flow around a cylinder to steady-state, and analysed the results. Fig 2 shows the velocity slip at the cylinder surface as a function of angle

θ around the cylinder, starting from $\theta = 0°$ at the stagnation point. Bearing in mind that it is inevitable that $|\mathbf{U}| \to 0$ as $\theta \to 0°$ and $\theta \to 180°$, the discrepancy between CFD and DSMC is quite appreciable between $30° < \theta < 110°$, although the peak slip velocity compares quite well. There is some difference in results using the Smoluchowski and Patterson temperature BCs due to appreciable differences in predicted temperature jump described later. The results with the Patterson temperature BC are marginally better.

Fig 3 shows the tangential velocity profile at $\theta = 90°$. The profile in the DSMC shows $|\nabla \mathbf{U}|$ begin to increase when $d/R \lessapprox 1$, reaching a level several times higher than in the CFD when $d \to 0$. Given such a difference in $|\nabla \mathbf{U}|$ in this region, discrepancy in calculated slip between the two methods is likely.

Fig 4 compares the fluid temperature along the cylinder wall in the DSMC and CFD simulations. The CFD with the Patterson's temperature BC compares far better with the DSMC than with the Smoluchowski temperature jump. Between $0° \geq \theta \geq 120°$, there is agreement in surface temperature between the results with Patterson's BC and DSMC to within $\pm 10\%$. The Smoluchowski BC predicts surface temperatures that are $\sim$100% too high.

The inaccuracy of the Smoluchowski BC is quite surprising, particularly at the stagnation point ($\theta = 0°$), where we estimate the local $Kn \approx 0.025$ based on a characteristic dimension $L = 2R$. Fig 5 shows the temperature profile along the geometry centre line between the stagnation point and a distance $2R$ upstream. Both CFD and DSMC predict similar normal temperature gradients $\nabla_{\mathbf{n}} T$ at the stagnation point, so reasonable prediction of the surface temperature would probably be expected by the temperature jump boundary condition models. However, while the Patterson BC gives good agreement near the surface, the Smoluchowski BC does not. The difference in results further upstream ($d/R > 0.5$) is typical, due to the inability of the NSF equations to replicate the diffuse behaviour exhibited in non-equilibrium flows.

At the highest point on the cylinder surface ($\theta = 90°$), there is an increase in the estimated local Kn to approximately 0.25. As figure Fig 6 shows, there is a larger discrepancy in $\nabla_{\mathbf{n}} T$ between the DSMC and CFD, and while the Patterson temperature BC gives better surface temperature prediction, its superiority over the Smoluchowski BC is less strongly evident than before.

In the wake of the cylinder, along the geometry centre line, the density is extremely low, driving the local Kn beyond 10. The DSMC results in Fig 7 show a rapid change in $\nabla_{\mathbf{n}} T$ near the cylinder surface that the Navier-Stokes model clearly does not predict in the CFD. However, the Patterson temperature BC predicts a wall temperature that, combined with the local $\nabla_{\mathbf{n}} T$ gives a match in T within $\pm 5\%$ to the DSMC results further downstream. The Smoluchowski BC, by comparison, produces a solution that is typically $\sim 20\%$ too high further downstream.

5 Mach 12.7 flow over a flat plate

We now consider a hypersonic flow of argon over a flat-plate at 0° angle of attack, as shown in Fig 8. The selected test case is that of a previous set of experiments [16]. The freestream parameters are $T_\infty = 64.5$ K, $\mathbf{U}_\infty = (1893.7, 0, 0)$ m/s, $p_\infty = 3.73$ Pa. These flow parameters

correspond approximately to Mach 12.7 and we can define a local $Kn = \lambda_\infty / x$ where x is the distance from the plate tip and $\lambda_\infty = 0.23$ mm is the free stream mean free path for this case. The plate surface is held uniform at $T_w = 292$ K.

The `rhoCentralFoam` application was used as in the Mach 10 cylinder case to solve to steady-state the Navier-Stokes equations with non-equilibrium BCs using the models and parameters described. Equivalent DSMC simulations were also conducted. The DSMC simulation used 1.58×10^6 equivalent particles, each representing 9.7×10^8 argon atoms. The mesh consisted of 75,600 square cells, each approximately 0.17×0.17 mm. The CFD simulations used a mesh of 28,000 cells that were graded from $\Delta y \approx 1.2$ mm at $y = 25$ mm to $\Delta y \approx 0.12$ mm at the plate surface ($y = 0$ mm) and $\Delta x \approx 0.15$ mm at the plate tip ($x = 0$ mm) to $\Delta x \approx 1.5$ mm at the outlet ($x = 55$ mm).

Fig 9 compares the fluid temperature along the plate surface. Near the plate tip, i.e. $x < 5$ mm, the DSMC and CFD results are clearly different. In the CFD, the fluid does not see the plate until it reaches the tip, when the shear stress begins to develop, although fairly slowly due to high slip. The formation of a shock, and the corresponding temperature jump across it, occurs slightly downstream of the plate tip, yielding the result we see in Fig 9 that T increases from T_∞ to a level downstream of the shock over 1-2 mm.

In the DSMC, however, the particles detect the presence of the plate slightly before the tip because a proportion of particles, reflected diffusely from the surface close to the tip, travel upstream and collide with incoming particles. The shock is established ~ 0.2 mm ahead of the plate tip, with the resulting deceleration in the flow causing a sharp rise in mean T of the particles behind the shock. The temperature of particles at the surface remains high until sufficient collisions have occurred with the plate surface at T_w.

The discrepancy between DSMC and CFD for $x < 5$ mm is perhaps not surprising, given that this region corresponds to $Kn > 0.05$ as defined above. For $x > 5$ mm the results are better, with the Patterson temperature BC giving better predictions of fluid temperature at the surface than the Smoluchowski BC. Fig 10 shows the profiles in T at $x = 25$ mm, from the plate surface through the viscous boundary layer to the edge of the shock. At the surface the Patterson BC predicts T to within 7%, whereas the Smoluchowski BC over-predicts T by $\sim 18\%$. The DSMC predicts a rise in T beyond 1000 K in the region 1-2 mm from the wall, which subsequently falls back to ~ 600 K at a wall distance of 3 mm. Beyond that, the comparison between the predicted temperatures from DSMC and CFD with the Patterson BC is very good, with DSMC exhibiting a more diffuse shock as expected. The over-prediction of surface temperature in the Smoluchowski BC propagates across the entire temperature profile.

Fig 11 shows similar profiles in T at $x = 50$ mm. Here the Patterson temperature BC predicts T at the surface to within 4% of the DSMC results, whereas the Smoluchowski BC over-predicts T by $\sim 16\%$. Again the DSMC exhibits a rapid rise in T beyond 1000 K near the wall, but beyond a wall distance of 6 mm the comparison between DSMC and CFD with the Patterson BC is excellent. Again, the over-prediction of surface temperature in Smoluchowski BC propagates across the entire temperature profile.

Fig 12 compares the predictions of velocity slip along the plate surface between the DSMC and CFD simulations. When the flow meets the plate tip, gas particles begin to collide with the wall and the mean velocity falls. Beyond a distance of approximately 10 mm from the

tip, the slip velocity stops decreasing rapidly when the rate of decrease of mean tangential velocity of particles due to surface collisions is matched by a similar rate of increase of mean tangential velocity by collisions from high-speed particles in the bulk. The main discrepancy between results from DSMC and CFD is in the level at which the velocity levels out, the slip velocity from DSMC is approximately 50% of that from the CFD.

Fig 13 shows the tangential velocity profiles at $x = 25$ mm. The comparison between CFD and DSMC is reasonable, with the profile using the Patterson temperature BC providing a closer match to the DSMC results than that using the Smoluchowski BC. The results are consistent with Fig 3 for the Mach 10 cylinder case, in which the DSMC predicts a steeper velocity gradient near the wall and a lower slip velocity at the surface.

6 Discussion

In this paper we have investigated non-equilibrium fluid dynamic BCs first by revisiting Patterson's derivation of model equations based on the moment method. We note first that the resulting equation for velocity slip reinforces previous arguments [3] that the conventional form of Maxwell's equation omits a term relating to surface curvature. Second, additional modifications to the BCs appear due to changes in the particle distribution function between incident and reflected particles, which appear in the equations through terms in ζ. For the Mach 10 cylinder case studied here, the modifications are unphysical since calculated values of ζ fall within a range that causes unboundedness (negative ρ or T) in the region near the cylinder surface at $\theta = 180°$. However, $\zeta = \zeta(\boldsymbol{\tau}, p)$ and $\boldsymbol{\tau}$ is calculated using the linear relationship of Eqn 5, which is inapplicable in this region of flow. It is possible that the inclusion of higher order terms for the stress will modify the flow itself and the calculation of ζ so that unboundedness does not occur.

In the simulations presented in this paper we ignored the modifications relating to ζ by setting $\zeta = 0$ in all equations. Our CFD simulations used a single equation for the velocity slip BC but two forms of equation were tested for the temperature jump BC. Perhaps surprisingly, Patterson's BC gave consistently better agreement with results from the DSMC comparison cases than the Smoluchowski BC did. The difference lies in an additional T_w/T in the respective model coefficients a_T of Eqns 27 and 30. This originates from Patterson's assumption that the denominator of the fraction on the right hand side of Eqn 25 is approximately unity. This assumption relies on $|\zeta| \ll 1$ and $|\mathbf{a} \bullet \mathbf{n}| \ll 1$, which is not true in this case. However, Patterson's analysis begins with the particle distribution function in Eqn 8 which represents a small deviation from a Maxwellian distribution and is only valid if the coefficients $\mathbf{a}, \mathbf{A}, \mathbb{A}$, and consequently ζ, are small compared to unity. In other words, the non-equilbrium BCs become invalid beyond a certain Kn, in the same way that the NSF equations themselves become invalid. Fig 4 certainly seems to confirm this, in which the Smoluchowski BC hugely over-predicts the temperature jump, to the extent that using an isothermal ($T = T_w$) condition would arguably be better.

One argument why Patterson's temperature BC generally outperforms the conventional Smoluchowski BC in the benchmark simulations presented in this paper is that the assumption used in arriving at Patterson's equation, based on a validity constraint of the underlying theory,

is effectively applying an additional model constraint for cases where the BC is used outside its normal range of applicability. The simulations performed here indicate strongly that the Smoluchoswki BC increasingly over-predicts temperature jump with increasing Kn, so scaling the model coefficient by T_w/T at least offers a heuristic solution that tends towards the original Smoluchowski condition in the limit $T \to T_w$.

Rarefied high-speed flows of practical interest exhibit different levels of thermodynamic non-equilibrium behaviour across the flow domain as the examples in this paper show. If these flows are solved using continuum CFD only, then it is beneficial that the governing equations and BCs do not, at least, produce unphysical or wildly inaccurate solutions within the more strongly non-equilibrium regions of flow for which the equations are not strictly applicable. For a temperature BC, Eqn 26 seems to offer an improvement over the conventional Smulochowski BC. Further work is needed to confirm this and there is perhaps also scope for exploring similar improvements to the velocity slip BC.

Acknowledgements

This research was supported by the UK's Engineering and Physical Sciences Research Council under grants EP/F014155/01 and EP/F005954/1. OPENFOAM is a registered trademark of OpenCFD Ltd. The authors thank Craig White at the University of Strathclyde for providing data from his DSMC simulations of the Mach 10 cylinder case, and the reviewers of this paper for their comments.

References

[1] J. C. Maxwell. On stresses in rarefied gases arising from inequalities of temperature. *Philosophical Transactions of the Royal Society of London*, 170:231–256, 1879.

[2] M. von Smoluchowski. Ueber wärmeleitung in verdünnten gasen. *Annalen der Physik und Chemie*, 64:101–130, 1898.

[3] D. A. Lockerby, J. M. Reese, D. R. Emerson, and R. W. Barber. Velocity boundary condition at solid walls in rarefied gas calculations. *Physical Review E*, 70:017303, 2004.

[4] Y. Sone, T. Ohwada, and K. Aoki. Temperature jump and Knudsen layer in a rarefied gas over a plane wall: Numerical analysis of the linearized Boltzmann equation for hard-sphere molecules. *Physics of Fluids A*, 1:363, 1989.

[5] F. Sharipov and D. Kalempa. Velocity slip and temperature jump coefficients for gaseous mixtures. I. Viscous slip coefficient. *Physics of Fluids*, 15:1800, 2003.

[6] H. Grad. On the kinetic theory of rarefied gases. *Communications on Pure and Applied Mathematics*, 2:331, 1949.

[7] G. N. Patterson. *Molecular Flow of Gases*. John Wiley and Sons, New York, USA, 1956.

[8] V. P. Shidlovskii. *Vvedenie v Dinamiku Razrezhennogo Gaza (Introduction of the Dynamics of Rarefied Gases)*. Nauka, Moscow, Russia, 1965.

[9] R. J. Vidal, T. C. Golian, and A. J. Bartz. An experimental study of hypersonic low-density viscous effects on a sharp flat plate. AIAA Physics of Entry into Planetary Atmospheres Conference, Cambridge, Mass., 63-435, 1963.

[10] R. N. Gupta, C. D. Scott, and J. N. Moss. Slip-boundary equations for multicomponent nonequilibrium airflow. NASA TP-1985-2452, 1985.

[11] A. J. Lofthouse, L. C. Scalabrin, and I. D. Boyd. Velocity slip and temperature jump in hypersonic aerothermodynamics. *Journal of Thermophysics and Heat Transfer*, 22:38–49, 2008.

[12] OpenCFD Ltd. `http://www.openfoam.com`, 2004.

[13] T. J. Scanlon, E. Roohi, C. White, M. Darbandi, and J. M. Reese. An open source, parallel DSMC code for rarefied gas flows in arbitrary geometries. *Computers and Fluids*, 39:2078–2089, 2010.

[14] G. A. Bird. The DS2V/3V program suite for DSMC calculations. In M. Capitelli, editor, *Rarefied Gas Dynamics*, pages 541–546. AIP Conference Proceedings 762, 2000.

[15] C. J. Greenshields, H. G. Weller, L. Gasparini, and J. M. Reese. Implementation of semi-discrete, non-staggered central schemes in a colocated, polyhedral, finite volume framework, for high-speed viscous flows. *Journal for Numerical Methods in Fluids*, 63:1–21, 2010.

[16] M. Becker. Flat plate flow field and surface measurements from merged layer into transition regime. In *6th International Symposium on Rarefied Gas Dynamics*, pages 515–528, 1970.

7 Figures

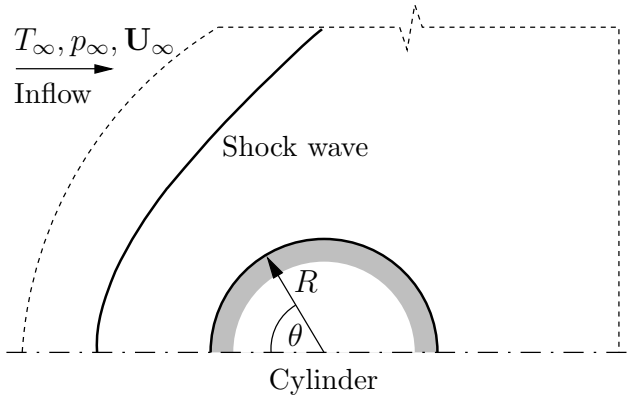

Figure 1: Mach 10 flow around a cylinder

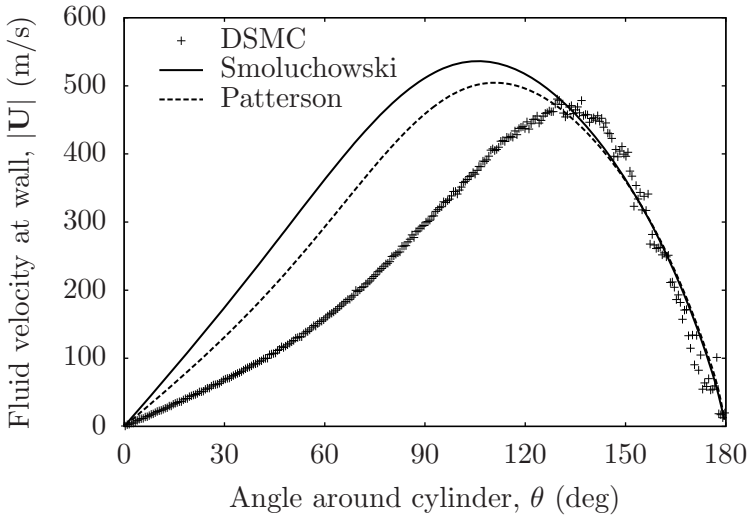

Figure 2: Slip velocity around cylinder surface

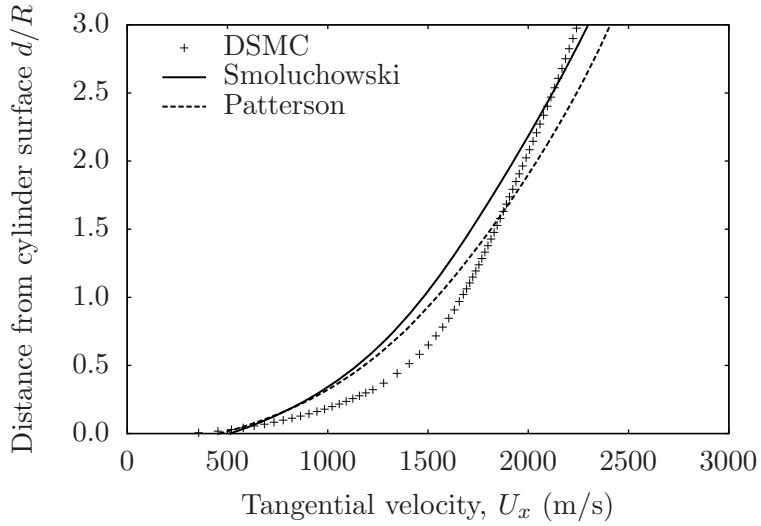

Figure 3: Tangential velocity along line normal to cylinder surface at $\theta = 90°$

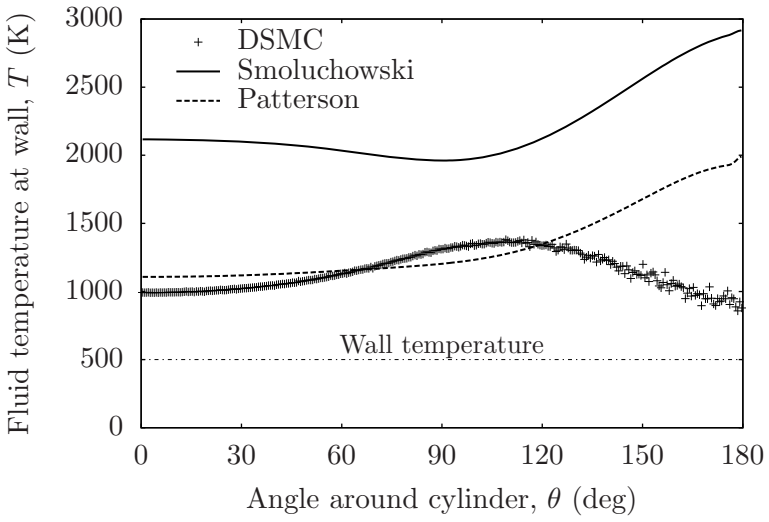

Figure 4: Temperature around cylinder surface

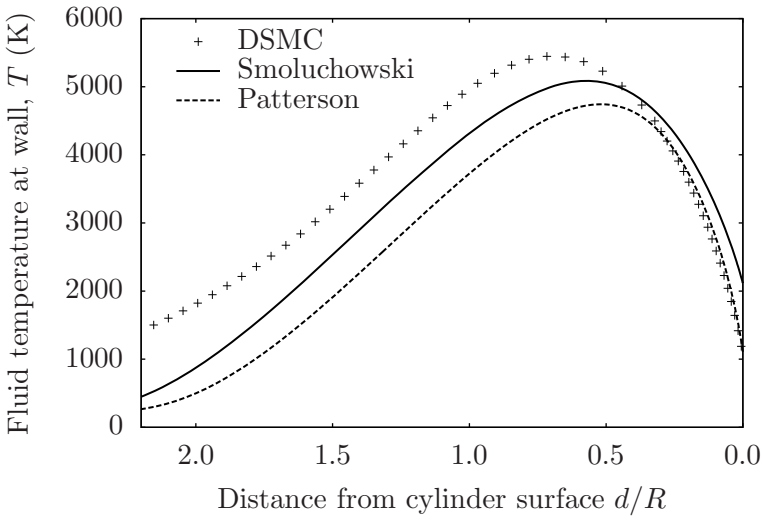

Figure 5: Temperature along line normal to cylinder surface at $\theta = 0°$ (note: left is upstream of cylinder; right is at the cylinder surface)

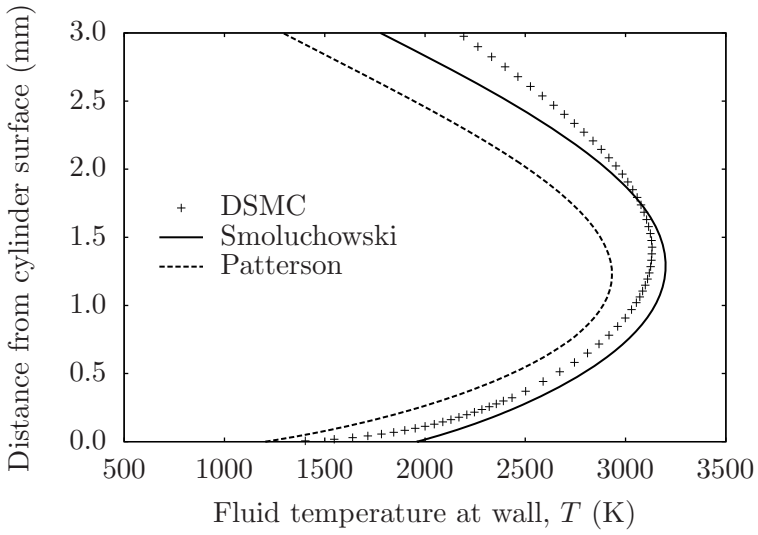

Figure 6: Temperature along line normal to cylinder surface at $\theta = 90°$

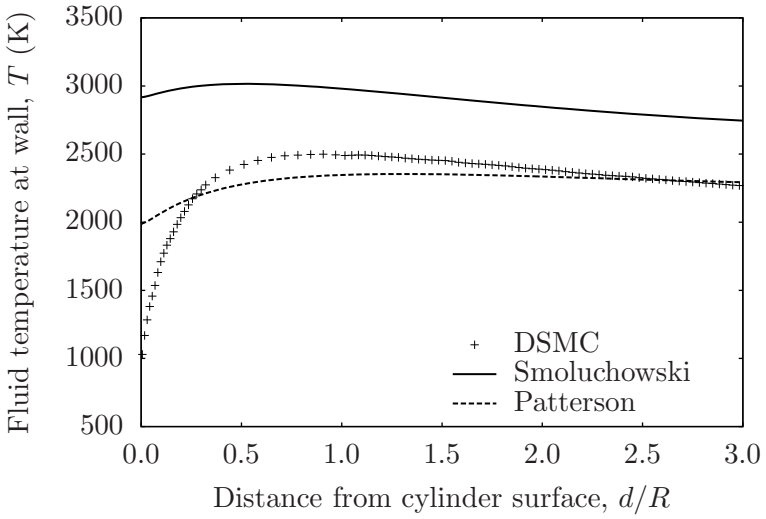

Figure 7: Temperature along line normal to cylinder surface at $\theta = 180°$ (left cylinder surface, right downstream of cylinder)

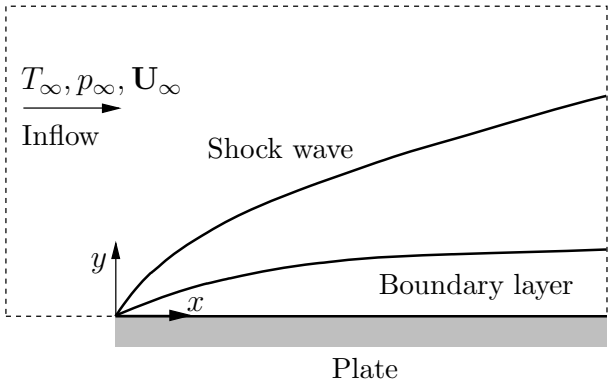

Figure 8: Laminar flow over a flat plate

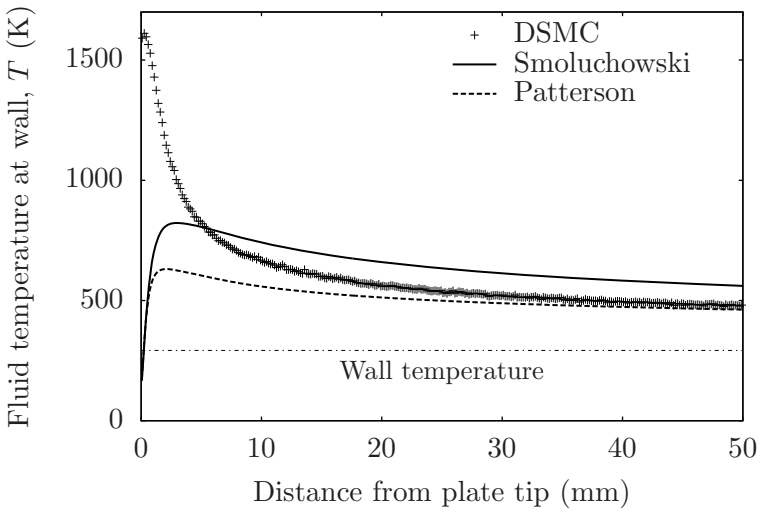

Figure 9: Temperature along surface of flat plate

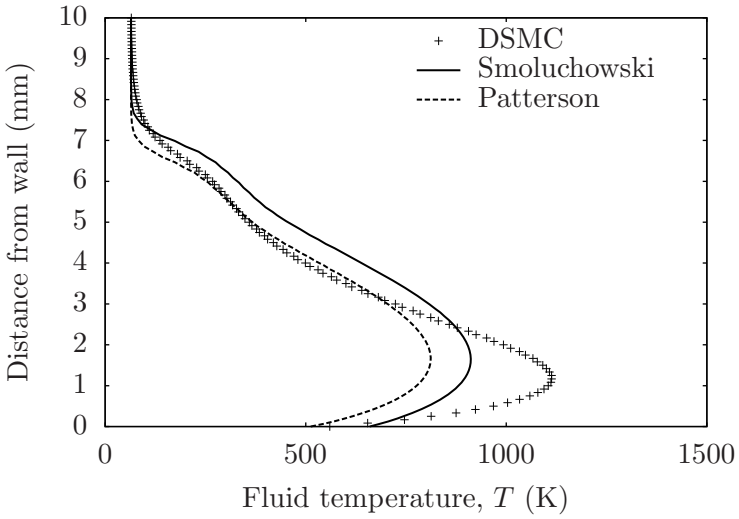

Figure 10: Temperature at cross section 25 mm from plate tip

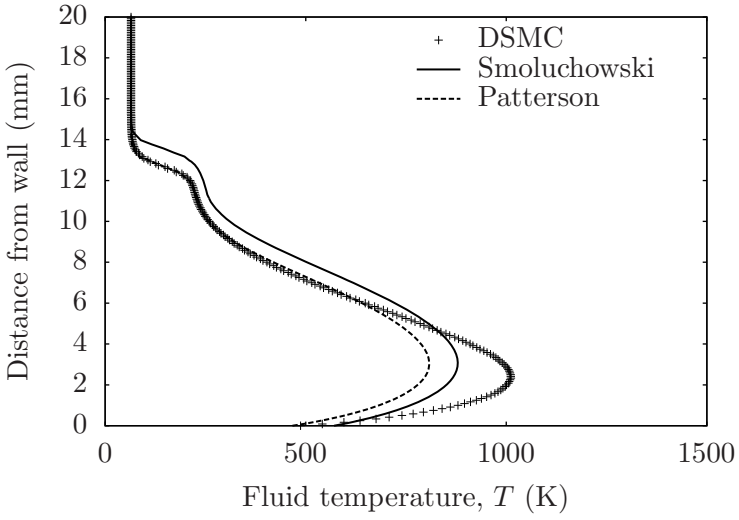

Figure 11: Temperature at cross section 50 mm from plate tip

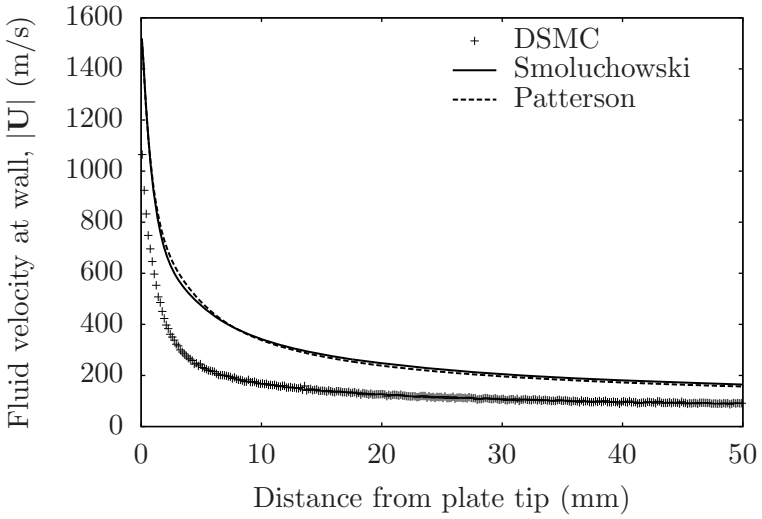

Figure 12: Velocity along surface of flat plate

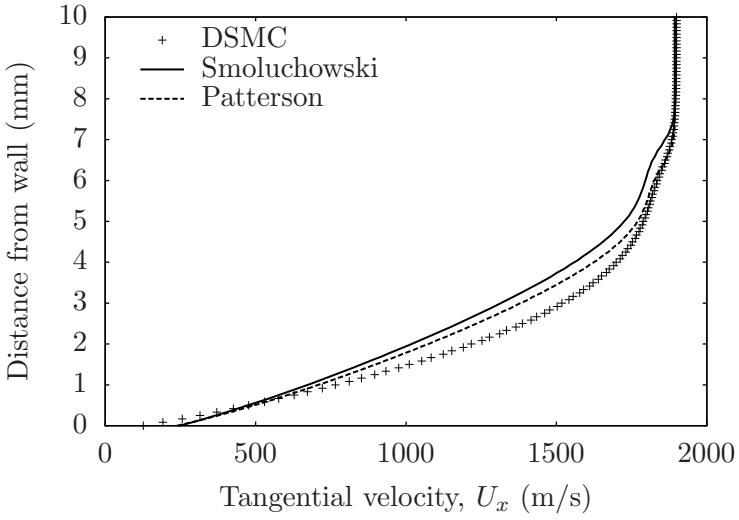

Figure 13: Tangential velocity at cross section 25 mm from plate tip